




GABA signaling enforces intestinal germinal center B cell differentiation

Yuxia Liao^{a,b,1} , Lijuan Fan^{b,1}, Peng Bin^{c,1}, Congrui Zhu^{b,1}, Qingyi Chen^b, Yepeng Cai^a, Jielin Duan^d, Qian Cai^a, Wei Han^e, Shizhen Ding^f, Xiangyu Hu^f, Yiran Zhang^a, Yulong Yin^{g,2}, and Wenkai Ren^{b,2}

Edited by Jason Cyster, HHMI, University of California, San Francisco, CA; received September 17, 2022; accepted September 29, 2022

Recent compelling results indicate possible links between neurotransmitters, intestinal mucosal IgA⁺ B cell responses, and immunoglobulin A nephropathy (IgAN) pathogenesis. Here, we demonstrated that γ -amino butyric acid (GABA) transporter-2 (GAT-2) deficiency induces intestinal germinal center (GC) B cell differentiation and worsens the symptoms of IgAN in a mouse model. Mechanistically, GAT-2 deficiency enhances GC B cell differentiation through activation of GABA–mammalian target of rapamycin complex 1 (mTORC1) signaling. In addition, IgAN patients have lower GAT-2 expression but higher activation of mTORC1 in blood B cells, and both are correlated with kidney function in IgAN patients. Collectively, this study describes GABA signaling–mediated intestinal mucosal immunity as a previously unstudied pathogenesis mechanism of IgAN and challenges the current paradigms of IgAN.

B cells | GABA | germinal center | IgA | IgAN

Characterized by the deposition of immunoglobulin A (IgA) in glomerular mesangium (especially for IgA1 immune complexes), IgA nephropathy (IgAN) is the most prevalent pattern of primary glomerulonephritis around the world. Although the exact pathogenesis of IgAN remains poorly understood, a multi-“hit” hypothesis is currently widely proposed and accepted to dissect the pathological processes of IgAN. Genetic or environmental factors induce increased amounts of circulatory Gd-IgA1 (incomplete glycosylation of IgA1 with galactose deficiency), which in turn acts as the autoantigen to trigger the production of autoantibody (anti-Gd-IgA1) to form pathogenic IgA immune complexes to deposit in the glomerular mesangium and induce renal inflammation and kidney injury (1–5). Thus, an increase in serum Gd-IgA1 level is the prerequisite for IgAN pathogenesis. Increasing evidence is showing that the mucosal immune system might be the major site for Gd-IgA1 synthesis (6–9). IgA⁺ plasma cells in the mucosal site would be misdirected to systemic sites, including bone marrow, and Gd-IgA1 would be secreted to promote the pathogenesis of IgAN. Therefore, a better understanding of mucosal IgA⁺ plasma cell fate decisions contributes to better knowledge of IgAN pathogenesis and helps to develop new therapeutic strategies for IgAN.

Increasing attention has highlighted the field of neuro-immune cross-talk because of its distinctive functions in maintaining physiological homeostasis and preventing inflammatory diseases (10–12). Anatomically, neuronal cells and immune cells share similar compartments in peripheral tissues, and communication and interaction between them are bridged by multiple molecular components, such as neurotransmitters, hormones, and cytokine factors (13–15). Notably, many neurotransmitters have critical importance in cell fate decisions of immune cells (16, 17). For example, our previous study found that γ -amino-butyric acid (GABA) regulates T helper type 17 (Th17) cell differentiation and macrophage polarization (18, 19). However, most studies focus mainly on macrophages and T cells, with relatively little attention on B cell subsets, especially for IgA⁺ plasma cells. Interestingly, previous genome-wide association studies have identified that the *Slc6a13* genetic variant affects kidney function and increases the risk of incident kidney diseases (20–22). *Slc6a13* encodes GABA transporter-2 (GAT-2) in humans and mice and participates in the uptake of GABA by cells (23). These compelling results suggest possible links between neurotransmitters, mucosal IgA⁺ B cell responses, and IgAN pathogenesis. Thus, we hypothesized that GAT-2 affects mucosal IgA⁺ cell responses, thereby affecting pathogenesis of IgAN.

Results

GAT-2 Is Expressed in B Cell Subtypes in Humans and Mice. To explore the possible roles of GAT-2 in B cell fate decisions, we analyzed the expression of GAT-2 in different subtypes of B cells from mice and humans (*SI Appendix, Fig. S1A*). We first

Significance

Immunoglobulin A nephropathy (IgAN) is characterized by the deposition of IgA in glomerular mesangium. Compelling results indicate possible links between neurotransmitters, intestinal mucosal IgA⁺ B cell responses, and IgAN pathogenesis; however the exact pathogenesis mechanisms of IgAN remain poorly understood. Here, we demonstrated that γ -amino butyric acid (GABA) transporter-2 (GAT-2) deficiency enhances germinal center B cell differentiation through activation of GABA–mammalian target of rapamycin complex 1 (mTORC1) signaling. In addition, IgAN patients have lower GAT-2 expression but higher activation of mTORC1 in blood B cells, and both are correlated with kidney function in IgAN patients. Collectively, this study describes GABA signaling–mediated intestinal mucosal immunity as a previously unstudied pathogenesis mechanism of IgAN.

Author contributions: W.R. designed research; Y.L., L.F., Q.C., Y.C., W.H., S.D., X.H., C.Z., and Y.Z. performed experiments; Y.L., Q. Cai, P.B., C.Z., and J.D. performed statistics analysis; Y.L., P.B., J.D., L.F., and C.Z. wrote the paper; Y.Y., and W. R. revised the paper and approved the final version of paper.

The authors declare no competing interest.

This article is a PNAS Direct Submission.

Copyright © 2022 the Author(s). Published by PNAS. This article is distributed under [Creative Commons Attribution-NonCommercial-NoDerivatives License 4.0 \(CC BY-NC-ND\)](https://creativecommons.org/licenses/by-nc-nd/4.0/).

¹Y.L., L.F., P.B., and C.Z. contributed equally to this work.

²To whom correspondence may be addressed. Email: yinyulong@isa.ac.cn or renwenkai19@scau.edu.cn.

This article contains supporting information online at [http://www.pnas.org/lookup/suppl/doi:10.1073/pnas.2215921119/-DCSupplemental](https://www.pnas.org/lookup/suppl/doi:10.1073/pnas.2215921119/-DCSupplemental).

Published October 24, 2022.

checked the mRNA expression of GAT-2 in naive B cells and germinal center (GC) B cells (CD45⁺B220⁺CD95⁺GL7⁺). Naive T cells were used as positive controls because our previous study demonstrated the expression of *Slc6a13* in naive T cells (18). *Slc6a13* was expressed in both naive B cells and GC B cells (SI Appendix, Fig. S1B), and the expression of *Slc6a13* in naive B cells was higher than in naive T cells, GC B cells, and lipopolysaccharide (LPS)-stimulated B cells (SI Appendix, Fig. S1 C and D). GAT-2 expressed in CD45⁺B220⁺ cells, CD45⁺B220⁺IgD⁺ cells, and GC B cells in mice was also validated by flow cytometry analysis (SI Appendix, Fig. S1E). B cell fate is highly shaped by other immune cells, such as innate immune cells (e.g., dendritic cells and macrophages) and Th cell subtypes, especially follicular Th cells (Tfh; CD45⁺CD4⁺CD185⁺PD-1⁺) and follicular regulatory T cells (Tfr; CD45⁺CD4⁺CD185⁺Foxp3⁺) (24, 25). As our previous studies found that innate immune cells (e.g., macrophages) and various types of Th cells (Th1, Th2, Th17, and regulatory T [Treg] cells) express GAT-2 (18, 19), we analyzed the expression of GAT-2 in Tfh cells in the current study. GAT-2 was also expressed in mouse CD45⁺CD4⁺ cells and Tfh cells (SI Appendix, Fig. S1 F and G). The expression of GAT-2 and other subtypes of GATs (GAT-1, GAT-3, and GAT-4) in B cells was also validated by immunoblotting (SI Appendix, Fig. S1H). Similarly, GAT-2 was also expressed in human blood CD45⁺CD3⁺, CD45⁺CD19⁺, and CD45⁺CD19⁺IgA⁺ cells (SI Appendix, Fig. S1I). Collectively, GAT-2 is expressed in B cells and those cells related to B cell fate decision.

GAT-2 Deficiency Promotes GC B Cells and IgA⁺ B Cells in Mouse Intestine. To further investigate the possible roles of GAT-2 in B cell fate decision, we established GAT-2-knockout (KO) mice (18) to delete GAT-2 in B cells and Tfh cells (SI Appendix, Fig. S1 E, G, and H). Then we compared the frequencies of B cell subtypes in the mesenteric lymph nodes (MLNs), spleen, and peripheral blood mononuclear cells (PBMCs) between GAT-2-KO mice and wild-type (WT) mice. In the MLNs, GAT-2-KO mice had higher frequencies of B220⁺ B cells and B220⁺IgA⁺ B cells but similar frequencies of IgM⁺IgD⁺ B cells and IgM⁺IgD⁺ B cells as WT mice (SI Appendix, Fig. S2 A–C). In the spleen, GAT-2-KO mice had comparable frequencies of IgM⁺IgD⁺ B cells, IgM⁺IgD⁺ B cells, and B220⁺IgA⁺ B cells as WT mice (SI Appendix, Fig. S2D). In PBMCs, GAT-2-KO mice had a lower frequency of B220⁺ B cells but higher frequencies of IgM⁺IgD⁺ B cells and B220⁺IgA⁺ B cells (SI Appendix, Fig. S2E). These results suggest that GAT-2 deficiency affects B cell profiles in a tissue-dependent manner.

To explore the possible roles of GAT-2 on intestinal mucosal B cell profiles, we analyzed the B cell profile in the ileum (Peyer's patches [PPs] included) and colon. Interestingly, although there was no difference in frequencies of IgM⁺IgD⁺ B cells and IgM⁺IgD⁺ B cells, GAT-2-KO mice had higher frequencies and numbers of GC B cells and IgA⁺ B cells (B220⁺IgA⁺ and B220⁺IgA⁺) in the ileum (Fig. 1 A–C). As the IgA⁺ B cells are capable of emerging from both the GC and extrafollicular pathways *in vivo* (26), we therefore further analyzed the percentage of CD95⁺GL7⁺ cells in IgA⁺ B cells to determine whether GAT-2 deficiency-dependent increases in IgA⁺ B cells are derived from the GC pathway. Notably, GAT-2-KO mice had a higher frequency and number of CD45⁺B220⁺IgA⁺CD95⁺GL7⁺ cells in the ileum (Fig. 1D and SI Appendix, Fig. S2F), indicating that the increased numbers of IgA⁺ B cells are from the GC. Notably, immunofluorescence analysis also showed a higher percentage of GC B cells in the

PPs of GAT-2-KO mouse ileum (Fig. 1E). A similar conclusion was also observed in the colon, where GAT-2-KO mice had higher frequencies and numbers of GC B cells, IgA⁺ B cells, and CD45⁺B220⁺IgA⁺CD95⁺GL7⁺ cells (Fig. 1 F–I and SI Appendix, Fig. S2F). Collectively, GAT-2 deficiency increases population of GC B cells and IgA⁺ B cells in the mouse intestine.

GAT-2 Deficiency Promotes GC B Cells and IgA⁺ B Cells in Mouse Intestinal PPs. Intestinal IgA-producing plasma cells can arise from the lamina propria and PPs. As GAT-2-deficient mice exhibited higher frequencies and numbers of CD45⁺B220⁺IgA⁺CD95⁺GL7⁺ cells (Fig. 1 D and I and SI Appendix, Fig. S2F), we therefore hypothesized that increased IgA⁺ B cells in GAT-2-deficient mice arise from PPs. To verify this hypothesis, we determined the subtypes of B cells in the ileal PPs. GAT-2-KO mice exhibited no difference in numbers of B220⁺ B cells and IgM⁺IgD⁺ B cells in the PPs (Fig. 2 A and B), but higher frequencies and numbers of CD95⁺GL7⁺ B cells and IgA⁺ B cells were observed in the ileal PPs (Fig. 2 C and D). After removal of PPs in the ileum, there was no difference in CD95⁺GL7⁺ B cells between the two groups (Fig. 2E).

Then, we tested the underlying reason why GAT-2 deficiency increases GC B cells by analyzing proliferation and apoptosis of GC B cells. Notably, there was no difference in proliferation between WT GC B cells and GAT-2-KO GC B cells as determined by Ki67 staining and 5-ethynyl-2'-deoxyuridine (EdU) uptake assay (SI Appendix, Fig. S3 A and B), and GAT-2-KO GC B cells even had a higher percentage of apoptosis than WT GC B cells (SI Appendix, Fig. S3C), indicating that GAT-2 deficiency induced GC B cells independent of apoptosis and proliferation. Studies have shown that GC B cell differentiation depends on Tfh cells, which promote antibody production and support antibody affinity maturation, while Tfr cells exert an inhibitory effect on Tfh cell-mediated antibody responses (27, 28). As both Tfh and Tfr cells collectively control the differentiation of GC B cells, we therefore analyzed the frequencies of Tfh and Tfr cells in ileal PPs. GAT-2-deficient mice exhibited lower frequencies of Tfr cells (Fig. 2F) and higher frequencies and numbers of Tfh cells (Fig. 2G), resulting in a higher Tfh/Tfr ratio in ileal PPs than in WT mice (Fig. 2H). Interestingly, GAT-2 deficiency promoted proliferation of both Tfr and Tfh cells and had no impact on apoptosis of these cells (SI Appendix, Fig. S3 D and E). The lower percentage of Tfr cells in GAT-2-KO mice suggests that GAT-2 deficiency may affect other underlying mechanisms for Tfr cells (29), including dendritic cell recognition, T cell receptor signaling, B cell interaction, and expression of factors such as Bcl6, Blimp-1, and interleukin-21, which requires further investigation. To further validate whether GAT-2 deficiency-induced IgA⁺ B cells depend on T cell–B cell interaction, we used signaling lymphocytic activation molecule–associated protein (SAP)-KO mice, which have T cell–intrinsic defects in T cell–dependent B cell responses (30, 31), to establish SAP and GAT-2–double KO mice (DKO) (Fig. 2I). SAP deficiency remarkably blocked the GAT-2 deficiency-induced increases in frequencies and numbers of GC B cells, IgA⁺ B cells, and CD45⁺B220⁺IgA⁺CD95⁺GL7⁺ cells (Fig. 2 J–M). In summary, GAT-2 deficiency promotes population of GC B cells and IgA⁺ cells in ileal PPs.

GAT-2 Deficiency Alters Intestinal IgA⁺ B Cell Responses and Intestinal Microbiota. To further investigate the impact of GAT-2 deficiency on intestinal IgA⁺ B cell responses, we analyzed intestinal secretory immunoglobulin A (SIgA) concentration. As expected, SIgA levels in the colon or colonic lumen of

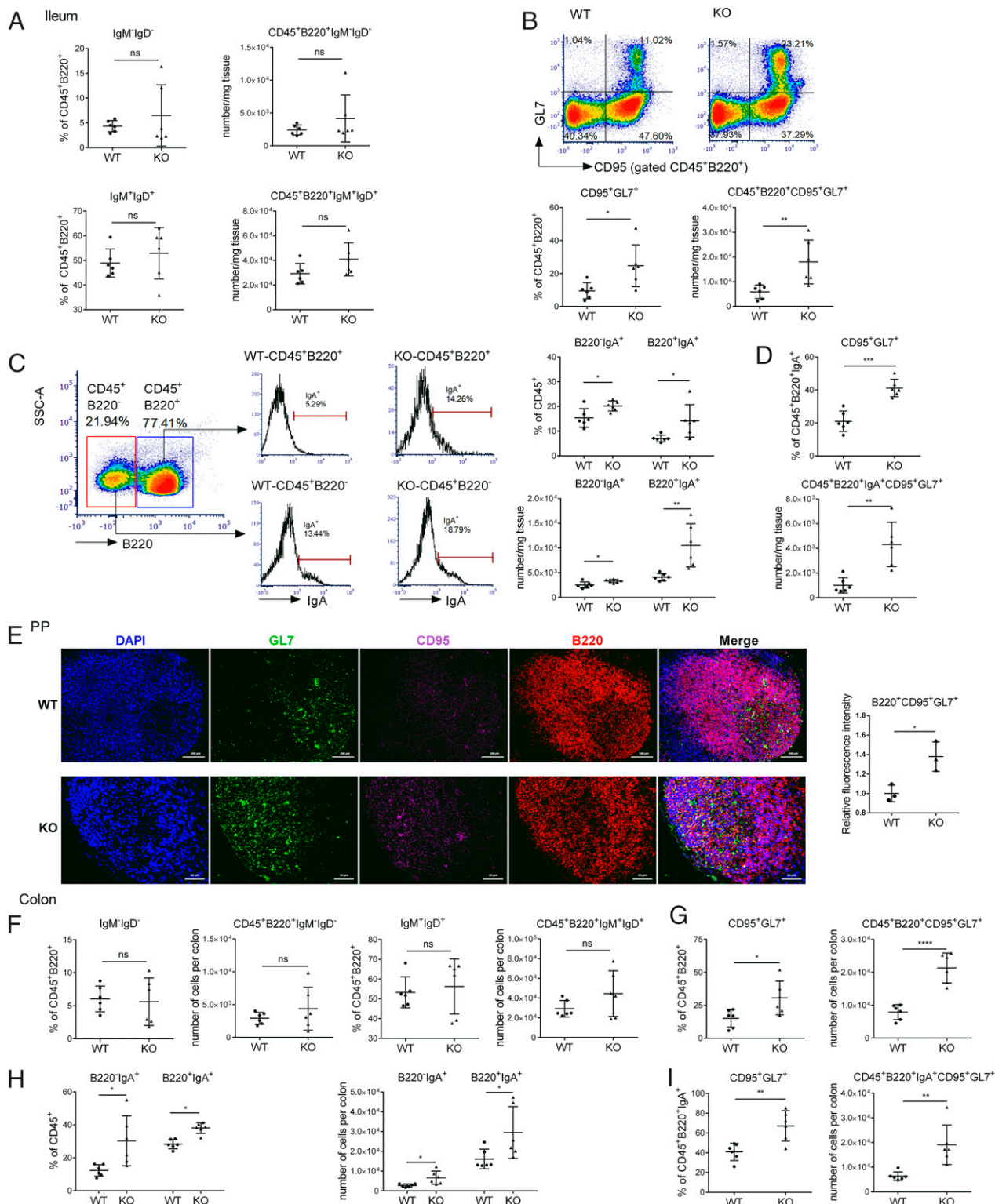


Fig. 1. GAT-2 deficiency promotes IgA⁺ B cells in mouse intestine. (A) Flow cytometry analysis of IgM⁻IgD⁻ cells and IgM⁺IgD⁺ cells in the ileum. Cells were pregated by CD45⁺B220⁺. Frequencies of IgM⁻IgD⁻ cells were analyzed by Mann-Whitney *U* test and are represented as means \pm SD. (B) Flow cytometry analysis of GC B cells (CD95⁺GL7⁺) in the ileum. Cells were pregated by CD45⁺B220⁺. (C) Flow cytometry analysis of B220⁺IgA⁺ and B220⁻IgA⁺ cells in the ileum. Cells were pregated by CD45⁺. (D) Flow cytometry analysis of CD95⁺GL7⁺ cells in the ileum. Cells were pregated by CD45⁺B220⁺IgA⁺. (E) Immunofluorescence analysis of GC B cells in the GCs of PPs (*n* = 3). (F) Flow cytometry analysis of IgM⁻IgD⁻ cells and IgM⁺IgD⁺ cells in the colon. Cells were pregated by CD45⁺B220⁺. Frequencies of IgM⁺IgD⁺ cells were analyzed by Mann-Whitney *U* test and are represented as means \pm SD. (G) Flow cytometry analysis of GC B cells (CD95⁺GL7⁺) in the colon. Cells were pregated by CD45⁺B220⁺. (H) Flow cytometry analysis of B220⁺IgA⁺ and B220⁻IgA⁺ cells in the colon. Cells were pregated by CD45⁺. (I) Flow cytometry analysis of CD95⁺GL7⁺ cells in the colon. Cells were pregated by CD45⁺B220⁺IgA⁺. Data were analyzed by unpaired *t* test and are represented as means \pm SD unless otherwise indicated; **P* < 0.05, ***P* < 0.01, ****P* < 0.001, and *****P* < 0.0001; ns, not significant. Data are pooled from two independent experiments with *n* = 5 to 6 mice (A–D, E, and F–I).

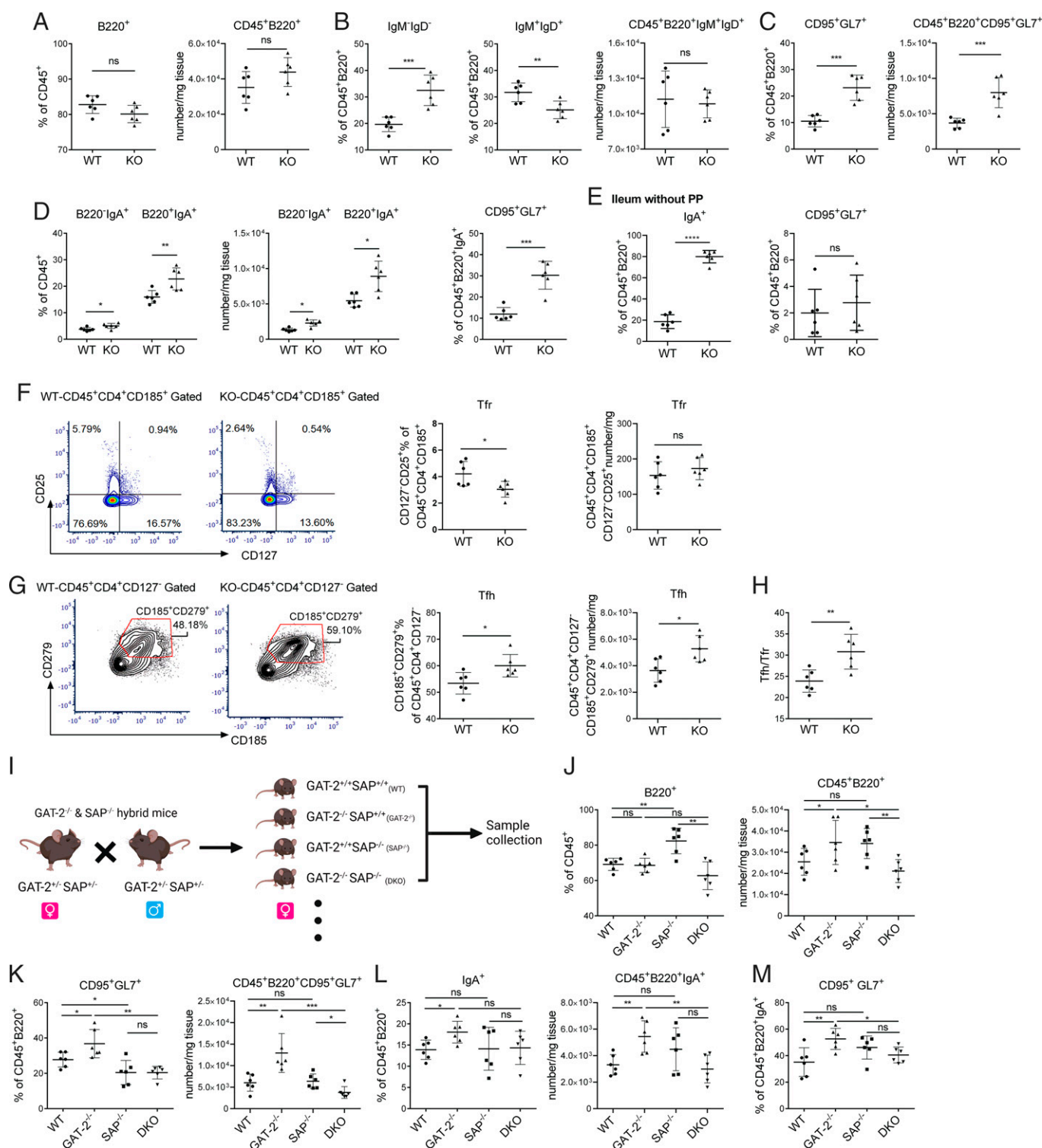


Fig. 2. GAT-2 deficiency promotes IgA⁺ B cells in mouse intestinal PPs. (A) Flow cytometry analysis of B220⁺ cells in the PPs. Cells were pregated by CD45⁺. (B) Flow cytometry analysis of IgM⁺IgD⁻ cells and IgM⁺IgD⁺ cells in the PPs. Cells were pregated by CD45⁺B220⁺. (C) Flow cytometry analysis of GC B cells in the PPs. Cells were pregated by CD45⁺B220⁺. (D) Flow cytometry analysis of B220⁺IgA⁺, B220⁺IgA⁺, and B220⁺IgA⁺CD95⁺GL7⁺ cells in the PPs. Cells were pregated by CD45⁺. (E) Flow cytometry analysis of IgA⁺ B cells and GC B cells in the ileum (PPs removed). Cells were pregated by CD45⁺B220⁺. (F) Flow cytometry analysis of Tfr cells (CD25⁺CD127⁻) in the PPs. Cells were pregated by CD45⁺CD4⁺CD185⁺. (G) Flow cytometry analysis of Tfh cells (CD185⁺CD279⁺) in the PPs. Cells were pregated by CD45⁺CD4⁺CD127⁺. (H) The ratio of Tfh to Tfr cells in the ileal PPs based on the data from E and F. (I) Flowchart for establishment of SAP GAT-2-DKO mice for J–M. F1 offspring of GAT2^{+/+}SAP^{-/-} hybrid mice were identified by genotype, and GAT2^{+/+}SAP^{+/+} (WT), GAT2^{-/-}SAP^{+/+} (KO), and GAT2^{-/-}SAP^{-/-} (DKO) mouse PP samples were collected for flow cytometry analysis. This figure was created using BioRender.com. (J) Flow cytometry analysis of B220⁺ cells. Cells were pregated by CD45⁺. (K) Flow cytometry analysis of GC B cells. Cells were pregated by CD45⁺B220⁺. (L) Flow cytometry analysis of IgA⁺ B cells. Cells were pregated by CD45⁺B220⁺. (M) Flow cytometry analysis of CD95⁺GL7⁺ cells. Cells were pregated by CD45⁺B220⁺IgA⁺. Data were analyzed by unpaired *t* test and are represented as means ± SD; **P* < 0.05, ***P* < 0.01, ****P* < 0.001, and *****P* < 0.0001; ns, not significant. Data are pooled from two independent experiments with *n* = 5 to 6 mice (A–M).

GAT-2-KO mice were higher than those in WT mice (*SI Appendix, Fig. S4A*). Moreover, we detected the expression of factors related to SIgA secretion in the colon, such as Th2 cytokines (IL-5, IL-6, and IL-13), transforming growth factor- β , and vasoactive intestinal peptide receptor 1 and 2 (VPAC1 and VPAC2) (32). GAT-2 deficiency significantly elevated the mRNA and protein levels of IL-13, VPAC1, and VPAC2 (*SI Appendix, Fig. S4 B and C*). Consistently, the percentage of IgA-coated fecal bacteria greatly increased in GAT-2-KO mice compared with in WT mice (*SI Appendix, Fig. S4D*), suggesting that GAT-2 deficiency promotes the intestinal IgA⁺ B cell responses.

Given that GAT-2 deficiency enhances intestinal SIgA levels, which markedly modulates the composition and diversity of intestinal microbiota, we therefore explored the influence of GAT-2 deficiency on intestinal microbiota. We analyzed the composition and diversity of intestinal microbiota between GAT-2-KO and WT mice. Although the detected operational taxonomic units were similar between GAT-2-KO and WT mice (*SI Appendix, Fig. S5A*), there was a significant difference in the structure of intestinal microbiota between GAT-2-KO and WT mice (*SI Appendix, Fig. S5 B and C*), suggesting that GAT-2 deficiency changes the intestinal microbiota composition. Notably, GAT-2 deficiency significantly increased the relative abundance of Ruminococcaceae but decreased the relative abundance of the Bacteroidales S24-7 group, Rikenellaceae, and Prevotellaceae (*SI Appendix, Fig. S5 D–F*).

The intestinal microbiota shapes host physiology through microbial metabolites. Therefore, we further tested whether GAT-2 deficiency impacts the metabolism of intestinal microbiota via metabolomics. The orthogonal partial least-squares discriminant analysis score plot exhibited a distinct separation between GAT-2-KO and WT mice (*SI Appendix, Fig. S5G*), and permutation tests verified the high accuracy and suitability of this model (*SI Appendix, Fig. S5H*). In total, 20 different metabolites were found in the feces, in which two metabolites (cholesterol and 4-cholesten-3-one) were up-regulated and 18 metabolites were down-regulated in GAT-2-KO mice compared with in WT mice (*SI Appendix, Fig. S5 I and J*). Notably, the GAT-2-KO and WT mice used for intestinal microbiota and metabolite analyses were littermates, which were kept in different cages after weaning; thus, the alterations in the intestinal microbiota and metabolites are largely from GAT-2 depletion-mediated change of intestinal IgA⁺ B cell responses.

GAT-2 Deficiency Induces GC B Cells Independent of Intestinal Microbiota. Since the mucosal or systemic microbiota have a profound influence in shaping B cell fate (33), and there is a remarkable difference in intestinal microbiota between GAT-2-KO and WT mice. Thus, we hypothesized that GAT-2 deficiency-mediated alteration of intestinal microbiota may also in turn contribute to the increased GC B cells and colonic SIgA production in GAT-2-KO mice. To verify this hypothesis, we treated the GAT-2-KO and WT mice with antibiotic mixtures (including streptomycin, ampicillin, gentamicin, and vancomycin) for 14 d to clear the intestinal microbiota (34). The protein levels of colonic SIgA, IL-13, VPAC1, and VPAC2 were comparable between GAT-2-KO and WT mice after antibiotic treatment (*SI Appendix, Fig. S6A*). Next, we cohoused GAT-2-KO and WT mice to normalize the intestinal microbial communities (35). In line with the data from antibiotic treatments, the concentrations of colonic SIgA, IL-13, VPAC1, and VPAC2 as well as the percentage of IgA-coated fecal bacteria showed no difference between cohoused GAT-2-KO and WT mice (*SI Appendix, Fig. S6 B and C*). These

data indicated that the intestinal microbiota has crucial roles in GAT-2 deficiency-induced colonic SIgA production in mice.

To determine whether increased GC B cells in GAT-2-deficient mice are also dependent on the intestinal microbiota, we analyzed B cell profiles from cohoused GAT-2-KO and WT mice (*SI Appendix, Fig. S7A*). The frequency of B220⁺ B cells was comparable between GAT-2-KO and WT mice (*SI Appendix, Fig. S7B*). However, higher frequencies and numbers of GC B cells and B220⁺IgA⁺ B cells remained in the ileal PPs from GAT-2-KO mice (*SI Appendix, Fig. S7 C–E*). To further rule out the involvement of the intestinal microbiota on GAT-2 deficiency-induced GC B cells, we also analyzed the frequencies of these types of B cells after 2 wk of cohousing with commercial WT mice (C57BL/6) and GAT-2-KO mice (*SI Appendix, Fig. S7F*). The frequencies of CD4⁺ T and B220⁺ B cells, IgM⁺IgD⁺ B cells, and IgM⁺IgD⁺ B cells were comparable between GAT-2-KO and commercial WT mice after cohousing (*SI Appendix, Fig. S7 G and H*). However, higher frequencies of GC B cells and B220⁺IgA⁺ B cells were found in the ileal PPs from GAT-2-KO mice (*SI Appendix, Fig. S7 I–K*). There was a difference between the changes in Tfh cells in GAT-2-KO mice and cohoused GAT-2-KO mice (Fig. 2G and *SI Appendix, Fig. S7L*), indicating the remarkable influence of the intestinal microbiota on intestinal Tfh cells (36). Notably, we still observed a higher Tfh/Tfr ratio in the ileal PPs from cohoused GAT-2-KO mice (*SI Appendix, Fig. S7L*).

Collectively, although the intestinal microbiota has crucial roles in GAT-2 deficiency-induced colonic SIgA production, GAT-2 deficiency induces GC B cells independent of the intestinal microbiota. Intestinal SIgA is secreted by IgA⁺ plasma cells via the complementary T cell-dependent (TD) and T cell-independent (TI) pathways, in which SIgA production through the TI pathway is the main pathway (37). This is a possible explanation for similar levels of intestinal SIgA between GAT-2-KO and WT mice after cohousing, even though GAT-2-KO mice have a higher percentage of GC B cells.

GAT-2 Deficiency Promotes GC B Cell Differentiation through the GABA-GABA Receptor (GABAR)–Mammalian Target of Rapamycin Complex 1 (mTORC1) Axis. The above results suggest that GAT-2 deficiency promotes IgA⁺ B cells via the TD pathway independent of the intestinal microbiota. To further rule out the involvement of the TI pathway in GAT-2 deficiency-induced IgA⁺ B cells, we conducted an experiment for plasmablast B cell differentiation *in vitro* and treated plasmablast B cells with TI LPS stimulation. Indeed, GAT-2 deficiency failed to increase the formation of plasmablast cells (CD138⁺B220⁺) from naive B cells after LPS stimulation without T cells *in vitro* (*SI Appendix, Fig. S8A*), further suggesting that GAT-2 deficiency affects GC B reaction and IgA⁺ B cells through the TD pathway. The differentiation of IgA⁺ B cells through the TD pathway requires the cognate cross-talk of CD40/CD40L signaling between Tfh cells and antigen-specific B cells. Considering that Tfh cells express GAT-2 (*SI Appendix, Fig. S1 F and G*), we hypothesized that GAT-2 deficiency promotes the differentiation of Tfh cells, resulting in higher numbers of Tfh cells in the PPs of GAT-2-KO mice (Fig. 2G). Thus, the effect of GAT-2 deficiency on differentiation of Tfh cells was explored *in vitro*. However, GAT-2 deficiency had little effect on Tfh cell differentiation from naive T cells *in vitro* (*SI Appendix, Fig. S8B*). Thus, the higher number of Tfh cells in GAT-2-KO mouse PPs might be from the increased proliferation of Tfh cells (*SI Appendix, Fig. S3D*).

Next, we explored the B cell-specific mechanism by which GAT-2 deficiency promotes GC B cell differentiation. GATs

regulate extracellular GABA concentration by transporting extracellular GABA into cells to curtail GABA signaling (18). In our previous study, we demonstrated that GAT-2 deficiency promotes differentiation of Th17 cells through GABA–GABAR–mTORC1 signaling (18), and mTORC1 signaling is an important signaling pathway involved in B cell fate decision (38, 39). Thus, we hypothesized that GAT-2 deficiency promotes GC B cell differentiation through GABA–GABAR–mTORC1 signaling. To validate this hypothesis, we isolated naive B cells and T cells from WT and GAT-2–KO mice to induce GC B cell differentiation *in vitro*. The WT naive B cells and WT naive T cells, WT naive B cells and GAT-2–KO naive T cells, GAT-2–KO naive B cells and WT naive T cells, GAT-2–KO naive B cells and GAT-2–KO naive T cells were cocultured and stimulated, respectively. The number of GC B cells was significantly increased when GAT-2–KO B cells were cocultured with either GAT-2–KO or WT T cells (Fig. 3*A*), suggesting that GAT-2 deficiency in B cells is the intrinsic factor for the increased GC B cell differentiation *in vitro*. Next, to test whether GABA–GABAR–mTORC1 signaling is activated in GAT-2–KO GC B cells *in vitro*, we first assessed the extracellular level of GABA in GC B cells. Although GAT-2 deficiency affected the expression of other GATs in B cells (*SI Appendix, Fig. S1H*), liquid chromatography–mass spectrometry (LC–MS) results revealed higher levels of extracellular GABA in GAT-2–KO GC B cells (Fig. 3*B*). GAT-2 deficiency had little effect on extracellular levels of other amino acids, except alanine and glutamine (*SI Appendix, Fig. S8C*). Then, we analyzed the protein abundance of GABAR and activation of mTORC1 signaling in B cells. GAT-2–KO B cells had higher protein abundance of GABA_AR and GABA_BR than WT B cells (Fig. 3*C*). Notably, the activation of mTORC1 and downstream signaling was also significantly elevated in GAT-2–KO B cells by flow cytometry analysis and immunoblotting (Fig. 3*D* and *E*). Consistently, there was higher activation of mTORC1 *in vivo* in GC B cells of GAT-2–KO mice (Fig. 3*F*). These results suggest that GAT-2 deficiency enhances GC B cell differentiation perhaps through GABA–GABAR–mTORC1 signaling.

To further validate whether the activation of GABA–GABAR–mTORC1 signaling is the key factor for increased GC B cell differentiation, three dosages of GABA (10, 50, and 250 μ g/mL) were supplemented to the cocultured WT naive B cells and naive T cells, and the frequency of GC B cells and the activation of mTORC1 in GC B cells were measured. GABA supplementation significantly increased the frequency of GC B cells (Fig. 3*G*) and induced the activation of mTORC1 in GC B cells (Fig. 3*H* and *I*). Next, we utilized GABAR inhibitors (bicuculline and GCP35348) and an mTOR inhibitor (rapamycin) to inhibit GABAR–mTORC1 signaling in GAT-2–KO GC B cells. As expected, these inhibitors significantly decreased the number of GC B cells and activation of mTORC1 in GC B cells (Fig. 3*J–L*). Collectively, these results indicate that GAT-2 deficiency promotes GC B cell differentiation through GABA–GABAR–mTORC1 signaling.

To further explore the B cell–specific roles of GAT-2 deficiency, we conducted an *in vivo* bone marrow transplantation assay. CD45.1 recipient mice were conditioned with 90 mg/kg busulfan to induce bone marrow immunosuppression, followed by syngeneic bone marrow transplantation from GAT-2–KO or WT CD45.2 donor mice. Bone marrow and PP cells were analyzed at 10 d after transplantation (Fig. 3*M*). There were significant increases in the percentages of GC B cells, IgA⁺ cells, and CD45⁺B220⁺IgA⁺CD95⁺GL7⁺ cells in the PPs of mice transplanted with bone marrow from GAT-2–KO donor

mice compared to mice transplanted with WT bone marrow cells (Fig. 3*N–P*). The KO group was transferred with GAT-2–deficient bone marrow cells rather than mixed WT and KO bone marrow cells. Thus, to further validate the B cell–specific roles of GAT-2 deficiency, we then conducted an adoptive transfer experiment. The WT or GAT-2–KO naive B cells and naive T cells were isolated, and WT naive B cells and WT naive T cells, WT naive B cells and GAT-2–KO naive T cells, GAT-2–KO naive B cells and WT naive T cells, GAT-2–KO naive B cells and GAT-2–KO naive T cells were transferred into *Rag1*^{−/−} mice by tail vein injection, respectively (Fig. 3*Q*). The numbers of GC B cells in the spleen and MLNs were analyzed on day 14 after transfer. The numbers of GC B cells in the spleen or MLNs were elevated in *Rag1*^{−/−} mice transferred with GAT-2–KO naive B cells and GAT-2–KO naive T cells (Fig. 3*R* and *S*). The activation of mTORC1 in splenic CD45⁺IgA⁺ cells was also higher in *Rag1*^{−/−} mice transferred with GAT-2–KO naive B cells and GAT-2–KO naive T cells (Fig. 3*T*). Collectively, GAT-2 depletion increases GC B cell differentiation through GABA–GABAR–mTORC1 signaling.

GABA Signaling Participates in the Pathogenesis of IgAN.

To further demonstrate the possibility of GABA–GABAR–mTORC1 signaling in increasing GC B cell numbers *in vivo*, we supplemented mice with GABA and then compared the GC B cells between GABA-supplemented and control mice (Fig. 4*A*). As expected, GABA supplementation increased the frequency of GC B cells in the PPs (Fig. 4*B*), despite having no effect on frequencies of IgM[−]IgD[−] B cells, IgM⁺IgD⁺ B cells, and B220⁺IgA⁺ B cells in the PPs (*SI Appendix, Fig. S9A*). Interestingly, GABA supplementation also increased the frequency of B220⁺IgA⁺ B cells in the blood (Fig. 4*C* and *SI Appendix, Fig. S9B*). Notably, the above effects were not observed when GAT-2–KO mice were supplemented with GABA (Fig. 4*D–F*). The higher extracellular GABA concentration and higher percentage of GC B cells in GAT-2–KO mice may overshadow the effect of GABA observed in WT mice. As GAT-2 deletion also lowered the abundance of GAT-1 and GAT-3 (*SI Appendix, Fig. S1H*) and inhibition of GAT-1 or GAT-3 can also elevate extracellular GABA concentration in mice, we conducted an *in vivo* GAT-1/GAT-3 inhibition assay (*SI Appendix, Fig. S9C*). Interestingly, either inhibition of GAT-1 or GAT-3 failed to increase the frequencies of GC B and IgA⁺ B cells (*SI Appendix, Fig. S9D* and *E*). These results suggested that GC B cell formation relies on extracellular GABA concentration, and GAT-2 is the major regulator to impair GABA uptake in B cells. To further validate the intrinsic roles of GABA–GABAR–mTORC1 signaling in GC B cells *in vivo*, we first inhibited GABA signaling by using bicuculline and CGP 35348 on WT mice (Fig. 4*G*). Treatment with bicuculline and CGP 35348 significantly decreased the frequency of GC B cells and inhibited the activation of mTORC1 signaling in GC B cells (Fig. 4*G*). We also inhibited GABA signaling in GAT-2–KO mice and found that bicuculline and CGP 35348 remarkably decreased the frequency of GC B cells and the activation of mTORC1 signaling in GC B cells (Fig. 4*H*).

IgA⁺ B cells are highly associated with the pathogenesis of IgAN, and we have observed higher percentages of IgA⁺ B cells in the blood of GAT-2–KO mice and GABA-supplemented mice (*SI Appendix, Fig. S2E* and Fig. 4*C*). Thus, we hypothesized that GABA signaling is associated with IgAN pathogenesis. To explore this hypothesis, we then constructed the IgAN model in GAT-2–KO mice and WT mice. These mice were stimulated by the combined administration of bovine serum

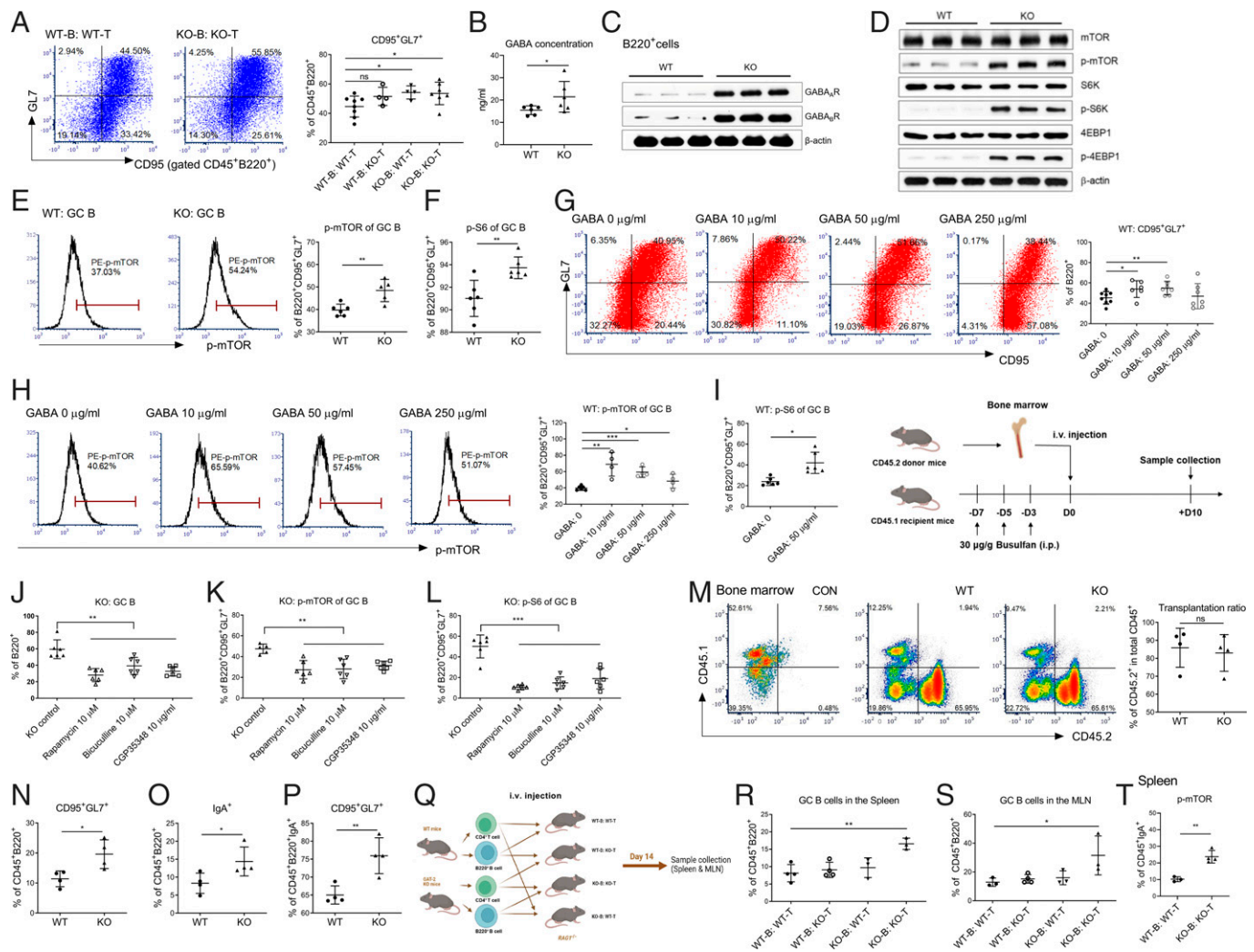


Fig. 3. GAT-2 deficiency promotes GC B cell differentiation through the GABA-mTORC1 axis. (A) Flow cytometry analysis of GC B cells (CD95⁺GL7⁺). Cells were pre-gated by CD45⁺B220⁺. Naive T cells and naive B cells were isolated from WT and GAT-2-KO mice, and the WT naive B cells and WT naive T cells, WT naive B cells and GAT-2-KO naive T cells, GAT-2-KO naive B cells and WT naive T cells, GAT-2-KO naive B cells and GAT-2-KO naive T cells were cocultured in B cell differentiation medium (containing Opti-MEM with anti-CD3 and anti-IgM μ -chain) for 72 h, respectively. Data are representative of two separate experiments with $n = 4$ to 6 replicates for each experiment. (B) GABA concentration in the supernatants of GC B cells was assessed by LC-MS ($n = 6$). (C) Protein abundance of GABA_AR and GABA_BR in B cells ($n = 3$). (D) Immunoblotting analysis of protein abundance of mTOR, phospho-mTOR (p-mTOR), S6K, p-S6K, 4EBP1, and p-4EBP1 in B cells ($n = 3$). (E) Flow cytometry analysis of p-mTOR abundance in GC B cells ($n = 5$ to 6). Cells were pre-gated by B220⁺CD95⁺GL7⁺. (F) Flow cytometry analysis of p-S6 abundance in vivo GC B cells of mouse PPs ($n = 6$). Cells were pre-gated by B220⁺. (G) Flow cytometry analysis of GC B cells after GABA supplementation. Figure I was created using BioRender.com. Cells were pre-gated by B220⁺. Data are representative of two separate experiments with $n = 6$ to 8 replicates for each experiment. (H and I) Flow cytometry analysis of p-mTOR and p-S6 abundance in GC B cells after GABA supplementation. Data are representative of two separate experiments with $n = 4$ to 5 replicates for each experiment. (J–L) Flow cytometry analysis of the percentage of GC B cells (J) and abundance of p-mTOR (K) and p-S6 (L) in GC B cells after GABA treatment (bicuculline and GCP35348) and mTOR inhibitor (rapamycin) treatment. Cells were pre-gated by B220⁺. Data are representative of two separate experiments with $n = 6$ replicates for each experiment. (M) Schematic diagram of in vivo bone marrow transplantation assay. CD45.1 recipient mice were conditioned with busulfan to induce bone marrow immunosuppression, followed by syngeneic bone marrow transplantation from GAT-2-KO or WT CD45.2 donor mice, separately, by tail vein injection. The transplantation ratio was calculated by percentage of CD45.2⁺ cells in total CD45⁺ bone marrow cells at 10 d after injection ($n = 4$). (N) Flow cytometry analysis of GC B cells in the PPs from mice treated as in M. Cells were pre-gated by CD45⁺B220⁺. (O) Flow cytometry analysis of IgA⁺ cells in the PPs from mice treated as in M. Cells were pre-gated by CD45⁺B220⁺. (P) Flow cytometry analysis of CD95⁺GL7⁺ cells in the PPs from mice treated as in M. Cells were pre-gated by CD45⁺B220⁺IgA⁺. (Q) Schematic diagram of in vivo lymphocyte transplantation assay. This figure was created using BioRender.com. WT naive B cells and WT naive T cells, WT naive B cells and GAT-2-KO naive T cells, GAT-2-KO naive B cells and WT naive T cells, GAT-2-KO naive B cells and GAT-2-KO naive T cells were transferred into the Rag1^{-/-} mice by tail vein injection, respectively, and CD95⁺GL7⁺ cells were analyzed at day 14 ($n = 3$ to 4); i.v., intravenous. (R and S) Flow cytometry analysis of GC B cells in the spleen (R) and MLN (S) from transferred Rag1^{-/-} mice. Cells were pre-gated by CD4⁺B220⁺. (T) Flow cytometry analysis of p-mTOR abundance in CD45⁺IgA⁺ cells from transferred mice ($n = 3$ to 4). Data are represented as mean \pm SD. Data between two groups were analyzed by unpaired t test (B, E, F, I, M–P, and T). Data in three or more groups were analyzed by one-way ANOVA with Bonferroni posttest (A, G, H, J–L, R, and S); * $P < 0.05$, ** $P < 0.01$, *** $P < 0.001$, and **** $P < 0.0001$; ns, not significant.

albumin (BSA), LPS, and CCL₄ for 7 wk to induce IgAN (Fig. 4I) (40). The weights of GAT-2-KO IgAN mice and WT IgAN mice were comparable in the first 4 wk, while the weights of GAT-2-KO IgAN mice were elevated in the last 3 wk (SI Appendix, Fig. S9F). The frequencies of B220⁺ and IgM⁺IgD⁺ B cells in most tissues were comparable between GAT-2-KO IgAN mice and WT IgAN mice (SI Appendix, Fig. S9 G–I). However, the frequencies of B220⁺IgA⁺ B cells in the blood, PPs, and spleen significantly increased in GAT-2-KO IgAN mice

(Fig. 4J). GAT-2-KO IgAN mice also had higher frequencies of GC B cells in the PPs (SI Appendix, Fig. S9H) and percentage of IgA-coated bacteria (Fig. 4K). Notably, GAT-2 deficiency aggravated inflammation and IgA deposition in the glomerulus of IgAN model mice (Fig. 4 L–O). Collectively, these results suggest that GABA signaling participates in the pathogenesis of IgAN.

IgAN Patients Exhibit Lower Expression of GAT-2. To validate our findings in our mouse model in IgAN clinics, we profiled

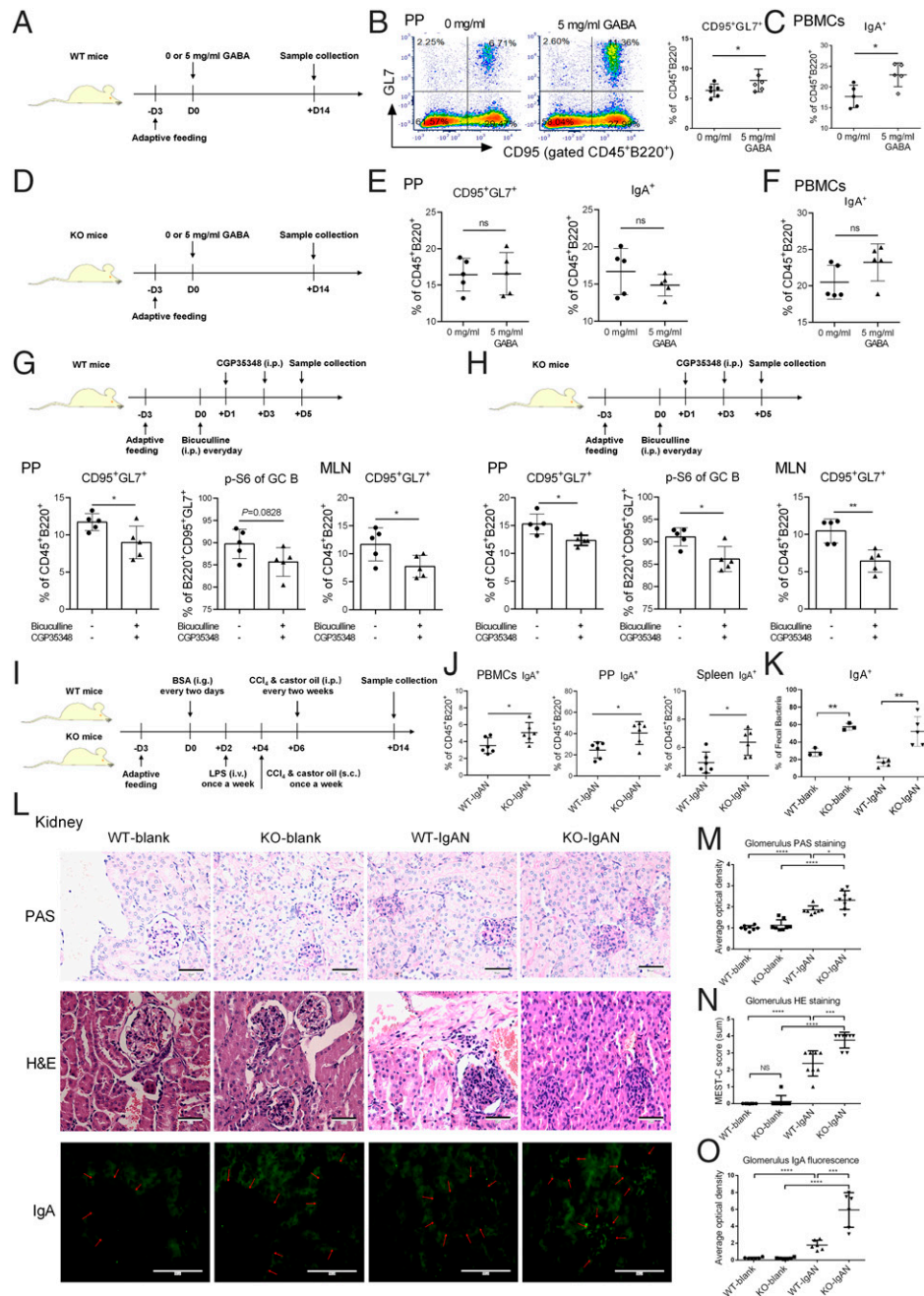


Fig. 4. GABA participates in IgAN pathogenesis. (A) Schematic diagram of experiment for GABA supplementation in mice. WT mice received GABA-supplemented (0 or 5 mg/mL GABA) water for 2 wk, and the PPs and blood samples were collected for flow cytometry analysis at day 14. (B and C) Flow cytometry analysis of GC B cells (CD95⁺GL7⁺) in the PPs (B) and IgA⁺ cells in PBMCs (C) from mice treated as in A. Cells were pregated by CD45⁺B220⁺ ($n = 5$ to 6). (D) Schematic diagram of the experiment for GABA supplementation in mice. KO mice received GABA-supplemented (0 or 5 mg/mL GABA) water for 2 wk, and the PPs and blood samples were collected for flow cytometry analysis at day 14. (E and F) Flow cytometry analysis of GC B cells (CD95⁺GL7⁺) and IgA⁺ cells in the PPs (E) and IgA⁺ cells in PBMCs (F) from mice treated as in D. Cells were pregated by CD45⁺B220⁺ ($n = 5$). (G) Schematic diagram of experiment for GABA inhibition in WT mice. WT mice were given bicuculline (intraperitoneally [i.p.], 7 mg/kg) daily for 4 d and CGP35348 (i.p., 30 mg/kg) at day 1 and day 3. PP and MLN samples were collected at day 5 for flow cytometry analysis of GC B cells (CD95⁺GL7⁺) in the PPs and MLNs and p-S6 in GC B cells of PPs. Cells were pregated by CD45⁺B220⁺. (H) Schematic diagram of experiment for GABA inhibition in GAT-2-KO mice. GAT-2-KO mice were given bicuculline (i.p., 7 mg/kg) daily for 4 d and CGP35348 (i.p., 30 mg/kg) at day 1 and day 3. MLN samples were collected at day 5 for flow cytometry analysis of GC B cells (CD95⁺GL7⁺) in the PP and MLN, and p-S6 in GC B cells of PPs. Cells were pregated by CD45⁺B220⁺. (I) Schematic diagram of experiment for IgAN in mice. The GAT-2-KO mice and WT mice were stimulated by the combined administration of BSA, LPS, and CCl₄ for 7 wk to induce IgAN, and the samples were collected at day 49; i.g., intragastric gavage; i.v., intravenous injection; s.c., subcutaneous injection; i.p., intraperitoneal injection. (J) Flow cytometry analysis of IgA⁺ cells in the blood, PPs, and spleen from WT IgAN and GAT-2-KO IgAN mice treated as in I ($n = 6$). Cells were pregated by CD45⁺B220⁺. (K) Percentage of IgA-coated fecal bacteria in mice treated as in I ($n = 3$ to 6). (L) The pathological differences (periodic acid-schiff (PAS) and the hematoxylin and eosin (H&E) staining) and IgA deposition (immunofluorescence confocal microscopy) in the glomerulus from mice treated as in I. The green plot represents deposited SIgA, and the red arrow describes the profile of the glomerulus ($n = 6$). (M–O) Statistical analysis of kidney PAS staining, HE staining score, and IgA immunofluorescence confocal microscopy. Data are represented as mean \pm SD and were analyzed by unpaired t test; * $P < 0.05$, ** $P < 0.01$, *** $P < 0.001$, and **** $P < 0.0001$; ns, not significant. Data were pooled from two independent experiments with $n = 5$ to 6 replicates in each experiment (B, C, E–H, J, K, and M–O).

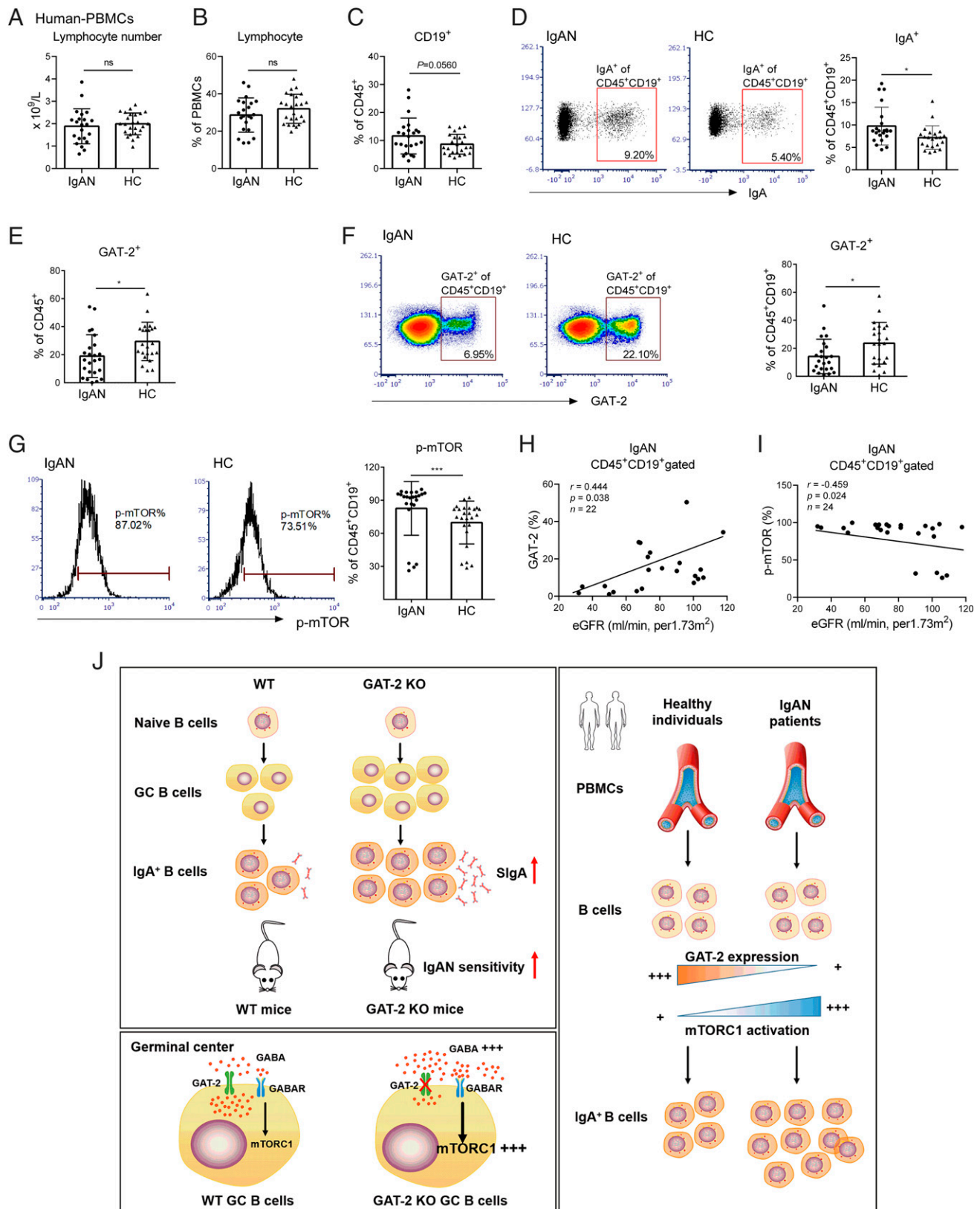


Fig. 5. GAT-2 expression in the B cells of IgAN patients. (A and B) Flow cytometry analysis of number and percentage of lymphocytes in the PBMCs between IgAN patients and healthy controls. (C) Flow cytometry analysis of CD19⁺ cells in the PBMCs of IgAN patients and healthy controls. Cells were gated by CD45⁺. (D) Flow cytometry analysis of IgA⁺ cells in the PBMCs of IgAN patients and healthy controls. Cells were gated by CD45⁺CD19⁺. (E and F) Flow cytometry analysis of GAT-2 expression in CD45⁺ cells (E) and CD45⁺CD19⁺ (F) cells from the PBMCs of IgAN patients and healthy controls. (G) Flow cytometry analysis of p-mTOR in CD45⁺CD19⁺ cells from the PBMCs of IgAN patients and healthy controls. (H and I) Correlation analysis of GAT-2 expression (H) and mTOR activation (I) with estimated glomerular filtration rate (eGFR). (J) The graphic summary of this study. GAT-2 deficiency promotes GC B cell differentiation through the GABA-mTORC1 axis, and IgAN patients exhibit lower GAT-2 expression but higher mTORC1 activation in blood B cells. The blood samples were collected from 24 IgAN patients (7 males and 17 females) and 25 healthy controls (11 males and 14 females). Data are represented as mean \pm SD. Data were analyzed by unpaired *t* test (A–E) or by Mann-Whitney *U* test (F and G); **P* < 0.05, ****P* < 0.01, *****P* < 0.001, and ******P* < 0.0001; ns, not significant.

GAT-2 expression in the blood lymphocytes from 25 healthy individuals and 24 IgAN patients. The percentages and numbers of blood lymphocytes and CD19⁺CD45⁺ PBMCs were largely comparable between healthy individuals and IgAN patients (Fig. 5 A–C). However, the IgAN patients showed higher percentages of IgA⁺ B cells (Fig. 5D). Then, we detected GAT-2 expression in CD45⁺ cells and B cells of the PBMCs. Interestingly, the expression of GAT-2 in CD45⁺ cells and B cells was decreased in IgAN patients compared with in healthy individuals (Fig. 5 E and F). The data from our mouse model demonstrated that GAT-2 inhibition induces activation of mTORC1 signaling to support the differentiation of GC B cells, and we speculated that this might mirror IgAN pathogenesis. Notably, mTORC1 activation was significantly higher in B cells of IgAN patients than in healthy individuals (Fig. 5G), suggesting that GAT-2 inhibition-induced activation of mTORC1 signaling may play crucial roles in IgAN pathogenesis. Notably, the expression GAT-2 in blood B cells was positively correlated with kidney function in IgAN patients, while the activation of mTORC1 in blood B cells was negatively correlated with kidney function in IgAN patients (Fig. 5 H and I). Collectively, IgAN patients exhibit lower GAT-2 expression but higher mTORC1 activation in blood B cells, and the expression of GAT-2 and activation of mTORC1 in blood B cells is correlated with kidney function in IgAN patients.

Discussion

In the current study, we have identified that GAT-2 deficiency elevates the frequencies of GC B cells and IgA⁺ B cells in the PPs and SIgA production in the colon, indicating that GAT-2 participates in the regulation of intestinal SIgA secretion. The differential trajectories of IgA⁺ plasma cells suggest that activated B cells successively undergo rapid proliferation and mutation or apoptosis in the GC, which ultimately differentiate into plasma cells or memory cells (41–43). However, GAT-2 deficiency-induced elevation of GC B cells and IgA⁺ B cells seems to be independent of proliferation and apoptosis of GC B cells. In addition to plasma cells, a proportion of selected GC B cells output from GC B cells differentiate into memory B cells (44). Unfortunately, it is unknown whether GAT-2 deletion targets memory B cell differentiation during GC responses. In addition, the influence of GAT-2 on other developmental stages of B cells, such as early lymphoid progenitor, common lymphoid progenitor, and pro-B and pre-B cells within bone marrow, remains to be further investigated.

GC responses are complex processes referring to the interaction of multiple cell types and signaling pathways. We found that GAT-2 deficiency impairs GABA uptake and activates mTORC1 signaling in GC B cells, which is essential for the differentiation of GC B cells. Consistent with this, previous research has described that lymphocytic choriomeningitis virus-infected *Rptor*-KO mice show lower frequencies and numbers of GC B cells in the spleen than WT mice (45). During the process of positive selection, mTOR signaling of light zone B cells is activated in a CD40-dependent manner, which promotes ribosome biogenesis and cell growth to support proliferative burst in the dark zone (46). Notably, the activation of mTOR signaling only increases anabolic capacity for dark zone proliferation rather than directly

acting on cell cycle progression (46). This finding appropriately interprets our observation that there are similar Ki67 percentages in GAT-2–KO and WT GC B cells. Moreover, intracellular nutritional status or activation of cellular immune signals modulates mTORC1 signaling to shape immune effector responses. For example, metformin decreases the frequencies of GC B cells and plasma cells through adenosine 5′-monophosphate (AMP)-activated protein kinase (AMPK)–mTOR–signal transducer and activator of transcription 3 (STAT3) signaling in the systemic lupus erythematosus model (47). Thus, it remains to be determined whether GAT-2 impacts cellular nutritional status or other signaling pathways to induce mTORC1 activation for mediating GC B cell differentiation.

Collectively, the GABAergic system plays a crucial role in shaping intestinal mucosal immunity. GAT-2 deficiency promotes GC responses through activating GABA–mTORC1 signaling (Fig. 5J). Importantly, GAT-2 deficiency-induced GC B cell differentiation participates in the pathological process of IgAN (Fig. 5J). Our findings have implications for further understanding IgAN pathogenesis and provide potential strategies for the early diagnosis and therapy of IgAN.

Materials and Methods

Mouse models, differentiation of GC B cells, Tfh cells, and plasmablast B cells *in vitro*, bone marrow transplantation, adoptive transfer of B and T cells, evaluation of IgA-coated bacteria by flow cytometry, cell isolation from the blood and intestinal tissues, flow cytometry, fluorescence-activated cell sorting, cell apoptosis analysis, 16S rRNA sequencing, nontargeted metabolomics, LC–MS analysis, Western blotting, enzyme-linked immunosorbent assay, immunofluorescence, GC B cell proliferation assay *in vivo*, RT-PCR, antibiotic treatment of mice, cohousing treatment of mice, GABA supplementation of mice, GAT-1/GAT-3 inhibition *in vivo*, GABAR inhibition *in vivo*, establishment of IgA nephropathy in mice, histological analysis of the kidney, collection of blood samples from IgAN patients, and statistical analyses are described in the [SI Appendix, Materials and Methods](#).

Data, Materials, and Software Availability. All study data related to this work are available in the paper and/or the [SI Appendix](#).

ACKNOWLEDGMENTS. This work was supported by National Key R&D Program of China (2021YFD1300700), Laboratory of Lingnan Modern Agriculture Project (NT2021005), and National Natural Science Foundation of China (31872365). SAP^{−/−} mice were a gift from Dr. Lili Ye (Army Medical University, Chongqing, China). We thank Sicheng Tao (School of Medicine, Nanjing Medical University), Yang Yang (College of Medicine, Yangzhou University), Guimei Kong (College of Medicine, Yangzhou University), Ming Yang (Department of Nephrology, Affiliated Hospital of Yangzhou University), Lei Wang (Department of Pathology, Affiliated Hospital of Yangzhou University), Hui Yang (Department of Nephrology, North Jiangsu People's Hospital), and Tianhua Jiang and Yun Sun (Health Management Centre, Affiliated Hospital of Yangzhou University) for collecting clinical samples.

Author affiliations: ^aSchool of Nursing & School of Public Health, Yangzhou University, Yangzhou, 225001, China; ^bCollege of Animal Science, South China Agricultural University, Guangzhou, 510642, China; ^cCollege of Veterinary Medicine, Yangzhou University, Yangzhou, 225001, China; ^dDepartment of Allergy and Clinical Immunology, the First Affiliated Hospital of Guangzhou Medical University, Guangzhou, 510120, China; ^eDepartment of Pathology, Affiliated Hospital of Yangzhou University, Yangzhou, 225003, China; ^fCollege of Medicine, Yangzhou University, Yangzhou, 225001, China; and ^gInstitute of Subtropical Agriculture, Chinese Academy of Sciences, Changsha, 410125, China

1. K. Kiryluk *et al.*, Discovery of new risk loci for IgA nephropathy implicates genes involved in immunity against intestinal pathogens. *Nat. Genet.* **46**, 1187–1196 (2014).
2. S. Taylor *et al.*, Phosphatidylethanolamine binding protein-4 (PEBP4) is increased in IgA nephropathy and is associated with IgA-positive B-cells in affected kidneys. *J. Autoimmun.* **105**, 102309 (2019).
3. K. Kiryluk, J. Novak, The genetics and immunobiology of IgA nephropathy. *J. Clin. Invest.* **124**, 2325–2332 (2014).

4. J. Floege, I. C. Moura, M. R. Daha, New insights into the pathogenesis of IgA nephropathy. *Semin. Immunopathol.* **36**, 431–442 (2014).
5. R. Magistroni, V. D. D'Agati, G. B. Appel, K. Kiryluk, New developments in the genetics, pathogenesis, and therapy of IgA nephropathy. *Kidney Int.* **88**, 974–989 (2015).
6. J. W. He, X. J. Zhou, J. C. Lv, H. Zhang, Perspectives on how mucosal immune responses, infections and gut microbiome shape IgA nephropathy and future therapies. *Theranostics* **10**, 11462–11478 (2020).

7. J. Floege, J. Feehally, The mucosa-kidney axis in IgA nephropathy. *Nat. Rev. Nephrol.* **12**, 147–156 (2016).
8. D. D. McCarthy *et al.*, Mice overexpressing BAFF develop a commensal flora-dependent, IgA-associated nephropathy. *J. Clin. Invest.* **121**, 3991–4002 (2011).
9. J. M. Chemouny *et al.*, Modulation of the microbiota by oral antibiotics treats immunoglobulin A nephropathy in humanized mice. *Nephrol. Dial. Transplant.* **34**, 1135–1144 (2019).
10. F. A. Pinho-Ribeiro *et al.*, Blocking neuronal signaling to immune cells treats streptococcal invasive infection. *Cell* **173**, 1083–1097 (2018).
11. A. J. Filiano *et al.*, Unexpected role of interferon- γ in regulating neuronal connectivity and social behaviour. *Nature* **535**, 425–429 (2016).
12. I. Gabanyi *et al.*, Neuro-immune interactions drive tissue programming in intestinal macrophages. *Cell* **164**, 378–391 (2016).
13. J. Chesné, V. Cardoso, H. Veiga-Fernandes, Neuro-immune regulation of mucosal physiology. *Mucosal Immunol.* **12**, 10–20 (2019).
14. S. S. Chavan, V. A. Pavlov, K. J. Tracey, Mechanisms and therapeutic relevance of neuro-immune communication. *Immunity* **46**, 927–942 (2017).
15. F. A. Pinho-Ribeiro, W. A. Verri Jr., I. M. Chiu, Nociceptor sensory neuron-immune interactions in pain and inflammation. *Trends Immunol.* **38**, 5–19 (2017).
16. S. A. Laped *et al.*, Intestinal epithelial Wnt signaling mediates acetylcholine-triggered host defense against infection. *Immunity* **48**, 963–978 (2018).
17. P. S. Olofsson *et al.*, $\alpha 7$ nicotinic acetylcholine receptor ($\alpha 7$ nAChR) expression in bone marrow-derived non-T cells is required for the inflammatory reflex. *Mol. Med.* **18**, 539–543 (2012).
18. W. Ren *et al.*, Slc6a13 deficiency promotes Th17 responses during intestinal bacterial infection. *Mucosal Immunol.* **12**, 531–544 (2019).
19. Y. Xia *et al.*, GABA transporter sustains IL-1 β production in macrophages. *Sci. Adv.* **7**, eabe9274 (2021).
20. A. Köttgen *et al.*, New loci associated with kidney function and chronic kidney disease. *Nat. Genet.* **42**, 376–384 (2010).
21. J. Raffler *et al.*, Genome-wide association study with targeted and non-targeted NMR metabolomics identifies 15 novel loci of urinary human metabolic individuality. *PLoS Genet.* **11**, e1005487 (2015).
22. N. Franceschini *et al.*, Generalization of associations of kidney-related genetic loci to American Indians. *Clin. J. Am. Soc. Nephrol.* **9**, 150–158 (2014).
23. A. Schlessinger *et al.*, High selectivity of the γ -aminobutyric acid transporter 2 (GAT-2, SLC6A13) revealed by structure-based approach. *J. Biol. Chem.* **287**, 37745–37756 (2012).
24. K. E. Huus, C. Petersen, B. B. Finlay, Diversity and dynamism of IgA-microbiota interactions. *Nat. Rev. Immunol.* **21**, 514–525 (2021).
25. V. Panneton, J. Chang, M. Witalis, J. Li, W. K. Suh, Inducible T-cell co-stimulator: Signaling mechanisms in T follicular helper cells and beyond. *Immunol. Rev.* **291**, 91–103 (2019).
26. S. A. Oracki, J. A. Walker, M. L. Hibbs, L. M. Corcoran, D. M. Tarlinton, Plasma cell development and survival. *Immunol. Rev.* **237**, 140–159 (2010).
27. J. Deng, Y. Wei, V. R. Fonseca, L. Graca, D. Yu, T follicular helper cells and T follicular regulatory cells in rheumatic diseases. *Nat. Rev. Rheumatol.* **15**, 475–490 (2019).
28. S. Hou *et al.*, FoxP3 and Ezh2 regulate Tfr cell suppressive function and transcriptional program. *J. Exp. Med.* **216**, 605–620 (2019).
29. F. Ribeiro, E. Perucha, L. Graca, T follicular cells: The regulators of germinal center homeostasis. *Immunol. Lett.* **244**, 1–11 (2022).
30. C. Kamperschroer, J. P. Dibble, D. L. Meents, P. L. Schwartzberg, S. L. Swain, SAP is required for Th cell function and for immunity to influenza. *J. Immunol.* **177**, 5317–5327 (2006).
31. A. Biram *et al.*, B cell diversification is uncoupled from SAP-mediated selection forces in chronic germinal centers within Peyer's patches. *Cell Rep.* **30**, 1910–1922 (2020).
32. M. Wu *et al.*, Glutamine promotes intestinal SIgA secretion through intestinal microbiota and IL-13. *Mol. Nutr. Food Res.* **60**, 1637–1648 (2016).
33. H. Li *et al.*, Mucosal or systemic microbiota exposures shape the B cell repertoire. *Nature* **584**, 274–278 (2020).
34. W. Ren *et al.*, Melatonin alleviates weanling stress in mice: Involvement of intestinal microbiota. *J. Pineal Res.* **64**, e12448 (2018).
35. R. Caruso, M. Ono, M. E. Bunker, G. Núñez, N. Inohara, Dynamic and asymmetric changes of the microbial communities after cohousing in laboratory mice. *Cell Rep.* **27**, 3401–3412 (2019).
36. F. Teng *et al.*, Gut microbiota drive autoimmune arthritis by promoting differentiation and migration of Peyer's patch T follicular helper cells. *Immunity* **44**, 875–888 (2016).
37. E. K. Grasset *et al.*, Gut T cell-independent IgA responses to commensal bacteria require engagement of the TACI receptor on B cells. *Sci. Immunol.* **5**, eaat7117 (2020).
38. A. Ortega-Molina *et al.*, Oncogenic Rag GTPase signaling enhances B cell activation and drives follicular lymphoma sensitive to pharmacological inhibition of mTOR. *Nat. Metab.* **1**, 775–789 (2019).
39. M. Yu *et al.*, PLC gamma-dependent mTOR signalling controls IL-7-mediated early B cell development. *Nat. Commun.* **8**, 1457 (2017).
40. X. Hu *et al.*, Respiratory syncytial virus exacerbates kidney damages in IgA nephropathy mice via the C5a–C5aR1 axis orchestrating Th17 cell responses. *Front. Cell. Infect. Microbiol.* **9**, 151 (2019).
41. R. A. Elsner, M. J. Shlomchik, Germinal center and extrafollicular B cell responses in vaccination, immunity, and autoimmunity. *Immunity* **53**, 1136–1150 (2020).
42. Y. Zhang, K. L. Good-Jacobson, Epigenetic regulation of B cell fate and function during an immune response. *Immunol. Rev.* **288**, 75–84 (2019).
43. A. M. Haberman, D. G. Gonzalez, P. Wong, T. T. Zhang, S. M. Kerfoot, Germinal center B cell initiation, GC maturation, and the coevolution of its stromal cell niches. *Immunol. Rev.* **288**, 10–27 (2019).
44. R. Shinnakasu *et al.*, Regulated selection of germinal-center cells into the memory B cell compartment. *Nat. Immunol.* **17**, 861–869 (2016).
45. B. Li *et al.*, Mammalian target of rapamycin complex 1 signalling is essential for germinal centre reaction. *Immunology* **152**, 276–286 (2017).
46. J. Ersching *et al.*, Germinal center selection and affinity maturation require dynamic regulation of mTORC1 kinase. *Immunity* **46**, 1045–1058 (2017).
47. S. Y. Lee *et al.*, Metformin suppresses systemic autoimmunity in *Roquinsan/san* mice through inhibiting B cell differentiation into plasma cells via regulation of AMPK/mTOR/STAT3. *J. Immunol.* **198**, 2661–2670 (2017).